A Radon Transform Based Approach for Extraction of Blood Vessels in Conjunctival Images

Reza Pourreza[1], Touka Banaee[2], Hamidreza Pourreza[3], and Ramin Daneshvar Kakhki[2]

[1] Electrical Engineering Department, Ferdowsi University of Mashhad, Iran
reza_pourreza@yahoo.com
[2] Ophthalmic Research Center, Khatam-Al-Anbia Hospital,
Medical Sciences University of Mashhad, Iran
{banaeet,DaneshvarR}@mums.ac.ir
[3] Computer Engineering Department, Ferdowsi University of Mashhad, Iran
hpourreza@um.ac.ir

Abstract. This paper proposes a local Radon transform-based algorithm for extraction of blood vessels in conjunctival images. This algorithm divides the image into overlapping windows and applies Radon transform to each window. Vessel direction in each window is found by detection of peak in Radon space. The proposed algorithm is capable of extracting blood vessels with a variety of widths. According to vessel width, extracted blood vessels are classified into some predefined classes and several statistics are computed for each class. Since the Radon transform is robust against noise, proposed algorithm is noise-independent and is more robust in comparison with other available algorithms.

1 Introduction

Eye is the only organ in the living subject where small vessels are directly visible, either in the conjunctiva, or in the retina. Diabetic retinopathy is a well known microvascular complication of diabetes. There is a standardized classification system for diabetic retinopathy and much work has been done in this field [1,2]. But there are few studies about disturbances of conjunctival vessels in diabetes and other diseases [3]. This is due to the great variability of the shape and course of conjunctival vessels. To detect any changes in the conjunctival vessels, there is a need for an objective measure. Clinical classification of conjunctival vessels is a difficult and observer-dependent task which may not be reproducible. This led us to think of vessel detection techniques in this regard.

Many researchers have invested in the vessel detection field; however, most works focus on retinal images [4,5]. The vessel detection techniques fall into four main categories: local operators, matched filters, vessel tracking and neural networks [6]. In this paper a Radon transform-based algorithm is proposed. The Radon transform is able to transform line-containing images into a domain where each line in the image gives a peak or a valley in that domain. The Radon transform is less sensitive to noise in the image than other line detectors, because the intensity fluctuations due to noise tend to be cancelled out by the process of integration [7]. Radon transform makes our algorithm more robust and less sensitive to noise than other proposed algorithms. In

A. Gelbukh and E.F. Morales (Eds.): MICAI 2008, LNAI 5317, pp. 948 – 956, 2008.

addition, the utilized technique for vessel detection simplifies the statistical analysis of the input conjunctiva image.

In the proposed algorithm conjunctiva image is firstly partitioned into some overlapping blocks. Local Radon transform is then applied to each block. The peak of sub-image in Radon space would be associated with the sub-vessel (if a sub-vessel lays in the sub-image). The projection angle which includes the peak is further analyzed for vessel presence validation and vessel width calculation. The extracted sub-vessels are then refined and the blocks are merged. The algorithm outputs some masks for different vessel widths. Each mask is associated with a special vessel width and is a map for those vessels with that specific width. The masks are analyzed for vessel classification and statistical analysis. The extracted statistical information is useful for medical purposes.

The rest of paper is organized in 6 parts as follow. Section 2 is *Image Partitioning* and explains the utilized partitioning method. Section 3 is *Local Radon Transform* which is concerned about local Radon transform and image analysis in Radon space. Section 4 is *Vessel Validation* and deals with validation of extracted sub-vessels and also width calculation of valid sub-vessels. Section 5 is *Vessel Refinement* and explains the method that extracted sub-vessels are compared with real ones to acquire better results. Section 6 is *Statistical Analysis* and in this section the output masks analysis for extracting statistical information, is discussed. The final section is *Results and Discussion*.

2 Image Partitioning

In order to extract blood vessels, sub-vessels should be extracted in local windows. The window size (n) has a direct effect on the extraction accuracy. A small/large n would lead to extract thin/thick vessels accurately while thick/thin vessels would not be extracted. A good combination of thin and thick vessels can be extracted by adjusting the n value. Another important parameter which affects the algorithm's accuracy is the windows overlapping, because non-overlapping windows extremely limit the quality of detected vessels. Thus in the proposed system a parameter $step$ is used which defines the adjacent windows overlapping ratio. Fig. 1 depicts the relation of $step$ and window size (n).

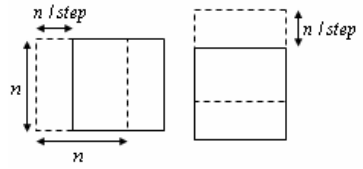

Fig. 1. Window size vs. Overlapping ratio

3 Local Radon Transform

The available conjunctiva images are mostly red-free, i.e. their R component in RGB color space equals zero. In the proposed algorithm, G component of sub-images are

selected for applying local Radon transform. The reason is the high contrast between blood vessels and image background in G component. G component is then complemented; this makes the vessels to be associated with peaks in Radon space (not valleys). In spite of the high contrast, we enhance the quality of sub-images before applying radon transform. Image enhancement i.e. histogram equalization improves the sub-image contrast and causes more discrimination between sub-vessels and conjunctiva's background and increases the total accuracy.

Local Radon transform is applied to the enhanced sub-image in the next step. The Radon transform of a continuous function $g(x, y)$ in 2-D Euclidian space is defined by (1)

$$R(\rho,\theta) = \int_{-\infty}^{+\infty}\int_{-\infty}^{+\infty} g(x, y)\delta(\rho - x\cos\theta - y\sin\theta)dxdy \tag{1}$$

where $\delta(x)$ is Dirac function. When $g(x, y)$ is an image, the integral boundaries would change to image dimensions as (2)

$$R(\rho,\theta) = \int_{0}^{Y}\int_{0}^{X} g(x, y)\delta(\rho - x\cos\theta - y\sin\theta)dxdy \tag{2}$$

where in our case both X and Y equal n. According to (1) and (2) the amplitude of projection in diagonal directions ($\theta = 45^{\circ}, \theta = 135^{\circ}, \rho = n\sqrt{2}$) is higher than other directions, thus the peak of Radon transform is more likely to happen in diagonal directions. To eliminate the diagonal effect, the input sub-image is firstly masked using a circle. The masking process is shown in fig. 2.

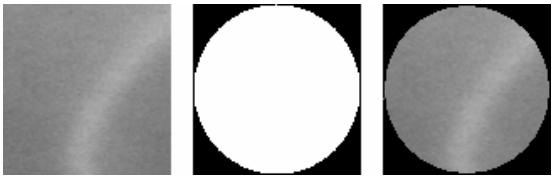

(a) (b) (c)

Fig. 2. Masking Process, a) sub-image, b) mask, c) masked sub-image

Then local Radon transform is applied to the masked image. As mentioned before, sub-vessels in sub-images are associated with peaks in Radon space; therefore at this stage peaks should be detected. However, the noise in the image moves the place of peaks or makes some fake peaks that would lead to false vessel detection. In order to remove the noise effect, the sub-image is filtered in radon space using a 3×3 mean filter. The peak and the corresponding projection angle are detected in the filtered Radon transform. The profile in which peak occurs, is a candidate that might contain a sub-vessel. This profile is further analyzed for validation of candidate sub-vessel.

4 Vessel Validation

An easy solution to the vessel validation problem is to compare the peak amplitude with a predefined threshold. However, this is a background-dependent solution, because the more/less bright background, the higher/lower peak amplitude. In our algorithm, effect of background and blood vessel on the peak amplitude are differentiated and then the comparison with the threshold is performed. In order to differentiate the background and vessel effects on peak amplitude, mean of sub-image is multiplied by window size (n) and then is subtracted from the profile as shown in (3)

$$P(i) = P(i) - n \times mean(subimage),\ i = 1,...,M \tag{3}$$

where P denotes profile and M is the number of bins in the profile.

Since the sub-image's mean is a good indicator of background, the multiplication of mean and window size would be the effect of background on the profile. The subtracted profile is background-free and in order to validate the presence of a sub-vessel in the candidate projection angle, profile's peak is normalized by division to the window size (n) and then compared with the threshold.

If the peak amplitude is bigger than threshold, the detected sub-vessel is verified and the algorithm should calculate sub-vessel's width. For this purpose the normalized profile is utilized. The normalized profile is the result of dividing the subtracted profile by window size. Fig. 3 depicts a normalized profile.

In fig. 3, i_p is the peak's index and is associated with the sub-vessel's centerline. The interval $[i_{\min}, i_{\max}]$ around i_p is the sub-vessel's area and $i_{\max} - i_{\min} + 1$ is using (4) to (7). In (4) to (7), α is a constant that equals 0.7 and P denotes profile.

$$i_{\max} > i_{\min} \tag{4}$$

$$P(i_{\max}) = \alpha \times P(i_p) \tag{5}$$

$$P(i_{\min}) = \alpha \times P(i_p) \tag{6}$$

$$w = i_{\max} - i_{\min} + 1 \tag{7}$$

Giving $i_{\min}$, $i_{\max}$, projection angle and window size, a mask is prepared which presents coarse sub-vessel's coverage area in the sub-image. For this purpose, on a black $n \times n$ block a white line is drawn which its angle equals projection age and its position is determined by $i_{\min}$ and $i_{\max}$ (so the width of drawn line equals w). A sample of local vessel mask is shown in fig. 4.

The local vessel mask is processed in the following sections for vessel map extraction and statistical analysis.

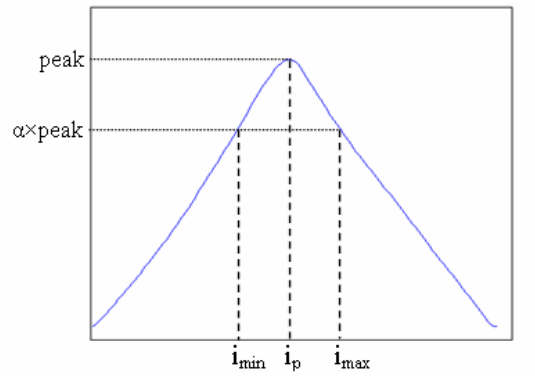

Fig. 3. Normalized Peak-Containing Profile

Fig. 4. Local Vessel Mask

5 Vessel Refinement

The output local vessel mask of *vessel validation* section represents sub-vessel which lays in the sub-image. However, it is not a good representation, because the drawn white line and the real sub-vessel may not fully cover each other and this phenomena decreases the quality of final detected vessel map and also disturbs the extracted statistical information. To improve the quality of extracted sub-vessels in the sub-image, the local vessel mask should be compared with real sub-vessels. For this purpose, the input sub-image is converted to a binary image which white pixels represent vessel area and black pixels represent background. A binarized sub-image is shown in fig. 5.

Fig. 5. Binary Sub-image

In order to determine the threshold for image binarization, the local vessel mask is compared with input sub-image and two gray level means are computed. First gray level mean (m_1) is the mean of those pixels' gray level in sub-image which their corresponding pixels in local vessel mask lay on white line. Second gray level mean (m_2) is the mean of those pixels' gray level in sub-image which their corresponding pixels in local vessel mask lay on black background. The binarization threshold equals mean of m_1 and m_2.

Essentially all white pixels in the acquired binary image are not associated with vessel pixels because image binarization is a noise-sensitive process. In our algorithm, the local vessel mask is compared with the binary sub-image to achieve a fine representation of sub-vessels and the result is named fine local mask. The comparison process is done through a logical AND as shown in (8).

$$FLM(i,j) = LVM(i,j)\,AND\,BSI(i,j) \qquad i,j = 1,...,n \tag{8}$$

where FLM , LVM and BSI denote fine local mask, local vessel mask and binary sub-image respectively. Fig. 6 shows the fine local mask.

Fig. 6. Fine Local Mask

So far, the input image was partitioned into sub-images; a sub-vessel was extracted from each sub-image (if there exist) and the output of algorithm for each sub-vessel was its fine representation (fine local mask) as well as its width (w). At last, fine local masks are merged to obtain the vessel map of the input image. In order to merge fine local masks, adjacent masks are put beside each other considering the overlapping ratio; on the overlapping region a logical OR is performed. The merging of two adjacent masks is shown in fig. 7.

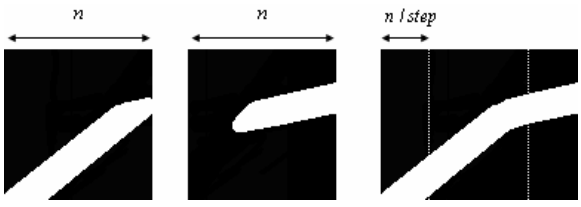

(a) (b) (c)

Fig. 7. Merging Process of adjacent masks, a) mask1, b) mask2, c) merged mask

Fig. 8 depicts a conjunctiva image which its vessel map is overlaid.

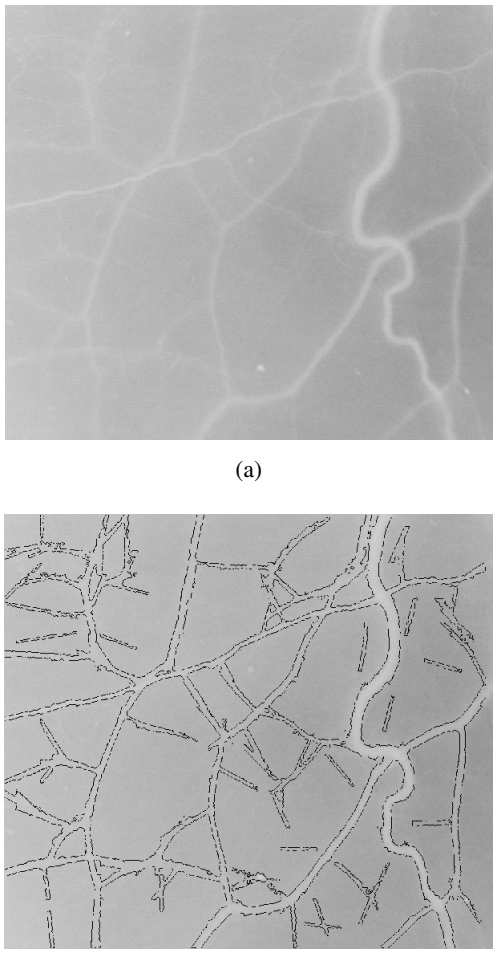

(a)

(b)

Fig. 8. Overlaid Vessel Map, a) G component of input image, b) overlaid detected vessels

Our algorithm is capable of extracting vessels whose widths vary over $[1, n-2]$ range. The merging process is done for each vessel width i.e. for each vessel width a vessel map is provided that contains those vessels with that specific width. Thus, $n-1$ vessel maps are prepared; one is the overall vessel map (m) and the others are associated with $n-2$ different vessel widths (m_i, $i = 1,...,n-2$ where i denotes vessel width,). The $n-1$ vessel maps are output to *statistical analysis* section.

6 Statistical Analysis

In this section, statistical information about the input conjunctiva image is extracted from the $n-1$ vessel maps. Statistical information includes: vessel width mean, vessel width variance and vessel density. All masks dimensions equal $H \times W$ where H and W denote image height and width respectively. In order to extract statistical information, the following $n-1$ statistics are computed using (9)

$$\begin{aligned} p &= \frac{1}{H \times W} \sum_{j=1}^{H} \sum_{k=1}^{W} s \times m(j,k) \\ p_i &= \frac{1}{H \times W} \sum_{j=1}^{H} \sum_{k=1}^{W} s \times m_i(j,k), \; i = 1,...,n-2 \end{aligned} \tag{9}$$

where m and m_i are defined in *Vessel Refinement* section, s is the scale factor in $\mu m / pixel$ and p denotes the number of white pixels (vessel pixels) to all pixels ratio in the corresponding mask.

Vessel density (d), which represents the density of vessels in the input image, equals p. Vessel width mean (μ) and variance (σ^2) are evaluated using (10) and (11) respectively.

$$\mu = \sum_{i=1}^{n-2} s \times i \times p_i \tag{10}$$

$$\sigma^2 = \sum_{i=1}^{n-2} (s \times i - \mu)^2 p_i \tag{11}$$

7 Results and Discussion

We applied our algorithm to 80 conjunctiva images. The input images dimensions were 768×864, window size (n) was 65, *step* was 3 and validation threshold was chosen 8.5. The extracted blood vessels were checked by a physician and the algorithm was evaluated subjectively. The acquired results demonstrate the high accuracy of our algorithm in vessel extraction and robustness against noise. As can be seen in fig. 8.b (which shows a sample result), our algorithm extracts both thin and thick vessels well even in low contrast regions.

References

1. Fowler, M.J.: Microvascular and Macrovascular Complications of Diabetes. Clinical Diabetes 26(2), 77–82 (2008)
2. Klein, R., Klein, B.E., Moss, S.E., Wong, T.Y.: Retinal vessel caliber and microvascular and macrovascular disease in type 2 diabetes: XXI: the Wisconsin Epidemiologic Study of Diabetic Retinopathy. Ophthalmology 114(10), 1884–1892 (2007)

3. Owen, C.G., Newsom, R.S.B., FRCOphth, Rudnicka, A.R., Ellis, T.J., Woodward, E.G.: Vascular Response of the Bulbar Conjunctiva to Diabetes and Elevated Blood Pressure. Ophthalmologhy 112(10), 1801–1808 (2005)
4. Kirbas, C., Quek, F.: A Review of Vessel Extraction Techniques and Algorithms. ACM Computing Surveys 36(2), 81–121 (2004)
5. Sang, N., Tang, Q., Liu, X., Weng, W.: Multiscale Centerline Extraction of Angiogram Vessels Using Gabor Filters. In: Zhang, J., He, J.-H., Fu, Y. (eds.) CIS 2004. LNCS, vol. 3314, pp. 570–575. Springer, Heidelberg (2004)
6. Estabridis, K., Defigueiredo, R.: Blood Vessel Detection via a Multi-window Parameter Transform. In: Proc. of CBMS 5960 (2006)
7. Zhang, Q., Couloigner, I.: Accurate Centerline Detection and Line Width Estimation of Thick Lines Using the Radon Transform. IEEE Transaction on Image Processing 24, 310–316 (2006)